H 2 O 2 Oxidation by Fe III –OOH Intermediates and Its Effect on Catalytic Efficiency

Juan Chen, Apparao Draksharapu, Davide Angelone, Duenpen Unjaroen, Sandeep Padamati, Ronald Hage, Marcel Swart, Carole Duboc, Wesley R. Browne

ACS Catalysis

Research Article

Cite This: ACS Catal. 2018, 8, 9665−9674

pubs.acs.org/acscatalysis

H_2O_2 Oxidation by Fe^{III}−OOH Intermediates and Its Effect on Catalytic Efficiency

Juan Chen,[†] Apparao Draksharapu,[†,#] Davide Angelone,[†,§] Duenpen Unjaroen,[†] Sandeep K. Padamati,[†] Ronald Hage,[‡] Marcel Swart,[§,∥] Carole Duboc,[⊥] and Wesley R. Browne*[,†]

[†]Molecular Inorganic Chemistry, Stratingh Institute for Chemistry, Faculty of Science and Engineering, University of Groningen, Nijenborgh 4, 9747AG, Groningen, The Netherlands

[‡]Catexel BV, BioPartner Center, Galileiweg 8, 2333BD Leiden, The Netherlands

[§]Institut de Química Computacional i Catàlisi (IQCC), Departament de Química, Universitat de Girona, Campus Montilivi, E17003 Girona, Catalonia, Spain

[∥]ICREA, Pg. Lluís Companys 23, 08010 Barcelona, Spain

[⊥]Departement de Chimie Moleculaire, Univ. Grenoble Alpes/CNRS, UMR-5250, BP-53, 38041 Grenoble Cedex 9, France

Supporting Information

ABSTRACT: The oxidation of the C−H and C=C bonds of hydrocarbons with H_2O_2 catalyzed by non-heme iron complexes with pentadentate ligands is widely accepted as involving a reactive Fe^{IV}=O species such as $[(N4Py)Fe^{IV}=O]^{2+}$ formed by homolytic cleavage of the O−O bond of an Fe^{III}−OOH intermediate (where N4Py is 1,1-bis(pyridin-2-yl)-*N*,*N*-bis(pyridin-2-ylmethyl)methanamine). We show here that at low H_2O_2 concentrations the Fe^{IV}=O species formed is detectable in methanol. Furthermore, we show that the decomposition of H_2O_2 to water and O_2 is an important competing pathway that limits efficiency in the terminal oxidant and indeed dominates reactivity except where only sub-/near-stoichiometric amounts of H_2O_2 are present. Although independently prepared $[(N4Py)Fe^{IV}=O]^{2+}$ oxidizes stoichiometric H_2O_2 rapidly, the rate of formation of Fe^{IV}=O from the Fe^{III}−OOH intermediate is too low to account for the rate of H_2O_2 decomposition observed under catalytic conditions. Indeed, with excess H_2O_2, disproportionation to O_2 and H_2O is due to reaction with the Fe^{III}−OOH intermediate and thereby prevents formation of the Fe^{IV}=O species. These data rationalize that the activity of these catalysts with respect to hydrocarbon/alkene oxidation is maximized by maintaining sub-/near-stoichiometric steady-state concentrations of H_2O_2, which ensure that the rate of the H_2O_2 oxidation by the Fe^{III}−OOH intermediate is less than the rate of the O−O bond homolysis and the subsequent reaction of the Fe^{IV}=O species with a substrate.

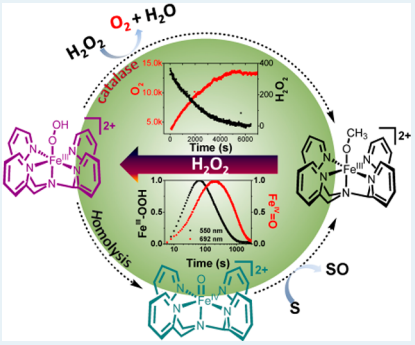

KEYWORDS: *iron, oxidation, peroxide, catalase, Raman spectroscopy, EPR spectroscopy*

Biomimetic analogues play a central role in understanding bioinorganic systems and enzymes, particularly in the identification of reactive intermediates and their role in catalytic processes.[1−4] In this context, high-valent iron oxo species (i.e., Fe^{IV}=O) have been studied intensely over the past decade,[5−9] especially since their first isolation and crystallographic characterization by Que and co-workers[10] in 2003. The synthetic non-heme Fe^{IV}=O complexes reported to date show a broad range of reactivity, including C−H oxidation,[7,11−14] with potencies comparable to those of non-heme and heme enzymes, such as Tau-D, and cytochrome P450.[15]

High-valent Fe^{IV}=O species are frequently invoked as the active species engaged in the oxidation of organic substrates by both heme and non-heme enzymes[5,7,16−18] and in biomimetic non-heme iron catalysts. The Fe^{IV}=O species that have been isolated to date are invaluable in determining their intrinsic reactivity, and their continuous regeneration under catalytic conditions, with H_2O_2 as terminal oxidant, is desirable in achieving turnover in the oxidative transformations that they engage in.

The formation of Fe^{IV}=O species upon homolytic O−O bond cleavage in the corresponding Fe^{III}−OOH complexes has been postulated to be a key step for the oxidation of organic substrates by nonheme iron catalysts with H_2O_2:[4,16,19] for example, in the oxidative cleavage of DNA by bleomycin−Fe^{III}−OOH.[20,21] Notably, in contrast to heme systems, where formation of Fe^{V}=O species is observed via heterolytic O−O bond cleavage (followed by oxidation of the porphyrin ligand to form compound **I**). Heterolysis of the O−O bond in low-spin non-heme iron(III)−hydroperoxy species is energetically unfavorable.[22−24]

However, to the best of our knowledge, this process (Fe^{III}−OOH → Fe^{IV}=O) was observed only recently for high-spin

Received: June 14, 2018
Revised: August 30, 2018
Published: September 6, 2018

DOI: 10.1021/acscatal.8b02326
ACS Catal. 2018, 8, 9665−9674

Fe^{III}−OOH species but has not yet been seen for low-spin Fe^{III}−OOH complexes.[25−29] Furthermore, the relatively low efficiency of non-heme iron complexes in alkane oxidations with an excess of H_2O_2, together with the known reactivity of Fe^{IV}=O species with H_2O_2,[30] casts doubt on the validity of this paradigm under catalytic conditions.[3]

The absence of evidence of the formation of Fe^{IV}=O species and loss of H_2O_2 through unproductive pathways (i.e., disproportionation) can be rationalized by assuming that the generated Fe^{IV}=O species either reacts with H_2O_2 or engages in, for example, C−H oxidation and hence the reaction of Fe^{IV}=O with H_2O_2 competes with its reaction with organic substrates. Indeed, Collins and co-workers have shown that the Fe^{III}(TAML) (TAML = tetraamidato macrocyclic ligand) system disproportionates H_2O_2 through a Fe^{IV}=O intermediate,[2] and of direct relevance to the present study, the complex $[(N4Py)Fe^{IV}{=}O]^{2+}$ (where N4Py is 1,1-bis(pyridin-2-yl)-*N*,*N*-bis(pyridin-2-ylmethyl)methanamine) was shown by Rohde and co-workers to react rapidly with H_2O_2 in acetonitrile.[30]

In the case of complexes based on pentadentate ligands, e.g., N4Py (Figure 1), the apparent stability of the Fe^{III}−OOH intermediate and absence of direct spectroscopic evidence for the formation of Fe^{IV}=O from it make it challenging to identify the actual mechanisms involved in substrate oxidation and H_2O_2 disproportionation.

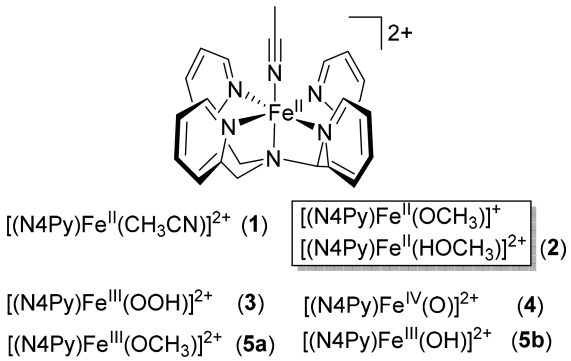

Figure 1. Structures of the complexes and intermediates discussed in the present study.

Here, using a combination of time-resolved UV−vis absorption, (resonance) Raman, and EPR spectroscopy and computational chemistry, we demonstrate that, contrary to expectations, the rate of O−O bond homolysis in $[(N4Py)Fe^{III}$−$OOH]^{2+}$ to form $[(N4Py)Fe^{IV}{=}O]^{2+}$ and a hydroxyl radical is much lower than the rate of H_2O_2 disproportionation observed under reaction conditions. We show that the Fe^{III}−OOH species is responsible for H_2O_2 decomposition. As a result, the efficiency of substrate oxidation is negatively affected by an increase in the steady-state H_2O_2 concentration, since formation of Fe^{IV}=O species is uncompetitive.

EXPERIMENTAL DETAILS

Synthesis. The ligand 1,1-bis(pyridin-2-yl)-*N*,*N*-bis(pyridin-2-ylmethyl)methanamine (N4Py),[31] $[(N4Py)Fe^{II}(CH_3CN)](ClO_4)_2$ (**1**),[21,31,32] and $[(N4Py)Fe^{IV}{=}O](PF_6)_2$ (**4**)[33] were prepared as reported previously. Commercially available chemicals were purchased from Sigma-Aldrich without further purification. All solvents used for spectroscopy were of UVASOL (Merck) grade. H_2O_2 was 50 wt % in H_2O from Sigma-Aldrich and was diluted in methanol as required. The concentration of H_2O_2 in methanol was confirmed by Raman spectroscopy (see Figure S7 for details).

Physical Methods. UV−vis absorption spectra were recorded with a Specord600 (Analytik Jena) spectrophotometer in 1 cm (unless stated otherwise) path length quartz cuvettes. Raman spectra at λ_{exc} 785 nm were recorded on a PerkinElmer Raman Station at room temperature. Raman spectra at 355 nm (10 mW at source, Cobolt Lasers) were acquired in a 180° backscattering arrangement. Raman scattering was collected by a 2.5 cm diameter plano convex lens (f = 7.5 cm). The collimated Raman scattering passed through an appropriate long pass edge filter (Semrock) and was focused by a second 2.5 cm diameter plano convex lens (f = 15 cm) into a Shamrock500i spectrograph (Andor Technology) 2399 L/mm grating blazed at 300 nm, acquired with an iDus-420-BU2 CCD camera (Andor Technology). The spectral slit width was set to 12 μm. Data were recorded and processed using Solis (Andor Technology) with spectral calibration performed using the Raman spectrum of acetonitrile/toluene, 50/50 (v/v).[34] EPR spectra (X-band, 9.46 GHz) were recorded on a Bruker ECS106 spectrometer in liquid nitrogen (77 K) or a Bruker EMX Nano spectrometer. Samples for measurements were transferred to a quartz 3 mm EPR tube (0.5 mL) and flash frozen in liquid nitrogen immediately, concurrent with monitoring by UV−vis absorption spectroscopy.

Computational Details. Computational studies were performed using ADF and QUILD,[35−37] as reported earlier.[38] Briefly, geometry optimization and frequency calculations were performed using the unrestricted density functional BP86-D_3[39−41] with a triple-ζ valence plus polarization basis set on iron combined with a double-ζ valence plus polarization on all other atoms (TDZP). Single-point energy calculations on these geometries were made with the S12g spin-state consistent functional[42,43] in a triple-ζ valence plus double polarization (TZ2P) basis set. Free energy (ΔG) corrections were obtained from the BP86-D_3 data and are corrected for zero point energy (ZPE); thermal and entropic corrections were made from frequency calculations at 298 K. The solvation energy was considered using methanol as a solvent with the COSMO solvation model as implemented in ADF.[44]

Caution! The drying or concentration of solutions that potentially contain H_2O_2 should be avoided. Prior to drying or concentrating, the presence of H_2O_2 should be tested for using peroxide test strips followed by neutralization on solid $NaHSO_3$ or another suitable reducing agent. In work with H_2O_2, suitable protective safeguards should be in place at all times due to the risk of explosion. In experiments where complex **2** is mentioned, it was prepared by dissolution of **1** in methanol (Figure S1).

Caution! In work with perchlorate salts, suitable protective safeguards should be in place at all times due to the risk of explosion. Perchlorate salts should be handled in small (milligram) quantities and used only where necessary.

RESULTS AND DISCUSSION

Typically, acetonitrile is the solvent of choice for the reaction of non-heme iron complexes with oxidants such as H_2O_2.[45] However, in acetonitrile, the formation of $[(N4Py)Fe^{III}$−$OOH]^{2+}$ (**3**) is observed only with a large excess (>50 equiv) of H_2O_2 and the subsequent formation of $[(N4Py)Fe^{IV}{=}O]^{2+}$ (**4**) has not been observed,[21] despite the fact that **4**, prepared independently, is itself stable in acetonitrile even at room temperature. This is in part due to the stability ($E_{1/2}$ = 1.2 V vs

DOI: 10.1021/acscatal.8b02326
ACS Catal. 2018, 8, 9665−9674

SCE) of $[(N4Py)Fe^{II}–NCCH_3]^{2+}$ (**1**) toward electron transfer oxidation and in part due to the high binding constant of the CH_3CN ligand in comparison with water or H_2O_2. In the present study methanol was chosen to circumvent the formation of such kinetically inert CH_3CN complexes. In methanol, the CH_3CN ligand of **1** exchanges immediately, to form **2** (which is either $[(N4Py)Fe^{II}–OCH_3]^{+}$or $[(N4Py)Fe^{II}–HOCH_3]^{2+}$ see the Supporting Information for a discussion), as manifested in a decrease and red shift in the near-UV and visible absorption bands (Figure S1).[32] The exchange of the methanol/methoxido ligand for water and H_2O_2 is relatively rapid in both the ferrous and ferric states (vide infra), which is central to enabling observation of other species involved in the reactions discussed and is in stark contrast to the slow ligand exchange seen for **1** in acetonitrile.

Reaction of 2 with Near-Stoichiometric H_2O_2 and Homolysis of O–O Bond of $[(N4Py)Fe^{III}\text{-}OOH]^{2+}$. Addition of 0.6 equiv of H_2O_2 to **2** results in immediate (<2 s) conversion to $[(N4Py)Fe^{III}–OCH_3)]^{2+}$ (**5a**) with its characteristic X-band EPR spectrum at g = 2.29, 2.12, and 1.96.[46] With 1.2 equiv of H_2O_2, $[(N4Py)Fe^{III}–OOH]^{2+}$ (**3**) is obtained in minor amounts by both UV–vis absorption and EPR spectroscopy (g = 2.16, 2.11, and 1.98;[21] Figure S2). Addition of 2 equiv of H_2O_2 to **2** results in the formation of $[(N4Py)Fe^{III}–OOH]^{2+}$ (**3**) (Figure 2) by ligand exchange over 50 s at room

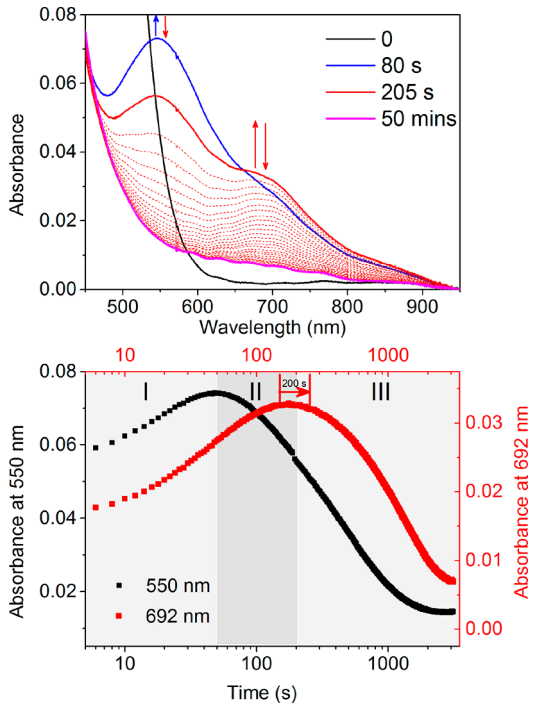

Figure 2. (top) UV–vis absorption spectrum of **2** (0.25 mM) in methanol before (black) and after addition of 2 equiv of H_2O_2 at 21 °C. (bottom) Corresponding change in absorbance over time at 550 and 692 nm. Path length: 2 cm.

temperature, reaching a maximum of 14% (based on the absorbance at 550 nm, Figure 2-I) before decreasing again over 1000 s. The decrease in absorbance at 550 nm (of **3**) proceeds concomitant with an increase in absorbance at 692 nm due to Fe^{IV}=O (**4**, Figure 2-II/III). Since **4** reacts rapidly (200 s) with even stoichiometric H_2O_2 (vide infra), its appearance indicates that the concentration of H_2O_2 in solution is already negligible by 80 s (vide infra). The absorbance at 692 nm remains almost constant over 200 s during the decay of **3**. The hydroxyl radical formed due to O–O bond homolysis will react with methanol (9.7×10^{-8} s^{-1}) to form a methoxy radical that can react with H_2O_2 or other species to yield either methanol or formaldehyde.

Once **3** has been fully consumed, the absorbance at 692 nm then decreases concomitant with the formation of more $[(N4Py)Fe^{III}–OCH_3]^{2+}$ (**5a**). These data are consistent with a prior equilibrium between **5a** and **3** followed by O–O bond homolysis to form **4**. Once sufficient H_2O_2 is consumed, the concentration of **4** is dependent only on the rate of its formation from **3** and the rate of its loss by reaction with methanol (vide infra). The rate of formation of **4** through homolysis of the O–O bond of $[(N4Py)Fe^{III}–OOH]^{2+}$ (**3**) under these conditions is low (<2.2×10^{-4} s^{-1}, vide infra), which is consistent with the reaction's endergonicity; calculated (see the Supporting Information) at 19.1 kcal mol^{-1}. The value is also consistent with the reported value calculated for the related homolytic cleavage in activated Fe–bleomycin.[18,23]

$$[(N4Py)Fe^{III}(OOH)]^{2+} \rightarrow [(N4Py)Fe^{IV}(O)]^{2+} + \dot{O}H$$
$$\Delta G = 19.1 \text{ kcal mol}^{-1} \quad (1)$$

Disproportionation of H_2O_2 by 3 in Methanol. Addition of excess H_2O_2 (>40 equiv) to **2** in methanol results in immediate oxidation to **5a** (i.e., a complete loss in absorbance at 450 nm within the mixing time, 2 s; Figure S3). The oxidation is followed by full conversion of **5a** to $[(N4Py)Fe^{III}–OOH)]^{2+}$ (**3**) over 5–10 s. The H_2O_2 concentration was monitored in real time by Raman spectroscopy. The second-order rate constant for the formation of **3** from **5a**, determined under pseudo-first-order conditions (2.5–50 mM H_2O_2, Figure 3 and Figure S4), is 10.5(±0.1) M^{-1} s^{-1} at 21 °C, consistent with the exothermicity (−10.2 kcal mol^{-1}) and low barrier for the exchange of the sixth ligand.

$$[(N4Py)Fe^{III}(OCH_3)]^{2+} + H_2O_2 \rightarrow [(N4Py)Fe^{III}(OOH)]^{2+} + CH_3OH$$
$$\Delta G = -10.2 \text{ kcal mol}^{-1} \quad (2)$$

EPR spectra of samples flash frozen to 77 K (Figure S5) immediately after addition of an excess of H_2O_2 show two well-resolved S = 1/2 signals, characteristic of **3** (major species) and **5a** (minor species). Samples, flash frozen after 18 min, show that the signals of **3** are diminished with the concomitant increase of in the signals of **5a**, and at ca. 50 min, the signals of **3** are absent, leaving only a more intense signal from **5a**.

Notably, both the maximum extent of formation of **3** and the time between addition of H_2O_2 and the start of the subsequent decrease in the absorbance of **3** are dependent on the initial concentration of H_2O_2 (Figure 3). These data indicate that H_2O_2 consumption is relatively similar to the rate of formation of **3** from **5a**. The rate of decrease of the absorbance due to **3** is independent of the initial H_2O_2 concentration (Figure S6), because the decay occurs only after essentially all of the H_2O_2 has been consumed, as confirmed by Raman spectroscopy (λ_{exc} 785 nm, Figure 4). Time-resolved Raman spectroscopy shows that the concentration of H_2O_2 decreases from t = 0 while the resonantly enhanced bands of **3** ($Fe^{III}–OOH$) at 632, 650, 670, and 798 cm^{-1} do not decrease in intensity until the signal (ν(O–O)) from H_2O_2 at 872 cm^{-1} has decreased to near-stoichiometric levels at least (i.e., below the limit of detection of ca. 10 mM, Figure S7).

DOI: 10.1021/acscatal.8b02326
ACS Catal. 2018, 8, 9665–9674

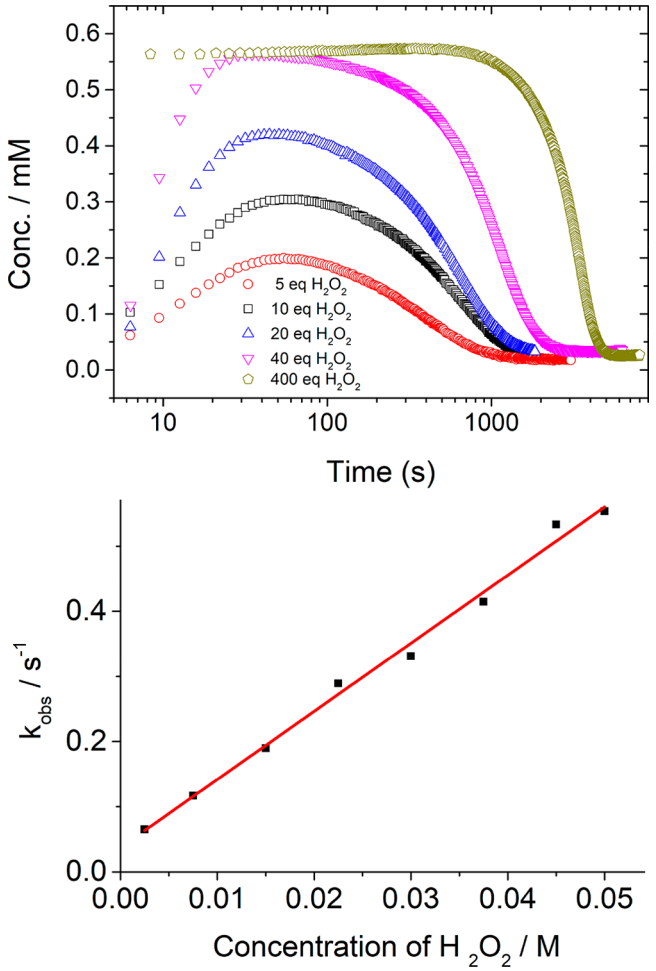

Figure 3. (top) Concentration of $[(N4Py)Fe^{III}–OOH]^{2+}$ (**3**, from absorbance at 550 nm) against log(time) for various amounts of H_2O_2 added (5 (red), 10 (black), 20 (blue), 40 (pink), and 400 (khaki) equiv) to **1** (0.56 mM) at 21 °C in methanol. (bottom) Pseudo-first-order rate constant k_{obs} for the formation of $[(N4Py)Fe^{III}–OOH)]^{2+}$ vs concentration of H_2O_2.

Regeneration of Fe^{III}–OOH and O_2 Evolution. For the absorption at 550 nm and its EPR signals, the characteristic Raman bands of **3** appear within the time resolution of the measurement (<60 s) upon addition of excess H_2O_2 and maintain their intensity until all H_2O_2 has been consumed. These data are consistent with the continuous regeneration of **3** from $[(N4Py)Fe^{III}–OR)]^{2+}$ (where R = H, CH_3) and H_2O_2. **3** is the resting state in the cycle, and the formation of **3** from **5a** is a rapid equilibrium prior to the rate-determining step in the reaction.

Headspace analysis by Raman spectroscopy (Figure 5 and Figure S8) confirms generation of O_2 at a rate corresponding to the rate of decrease of H_2O_2. Details for the quantification of O_2 generated are provided in section 3 of the Supporting Information.

The relation between the rate of consumption of H_2O_2 and concentration of **3** is apparent when H_2O_2 is present in excess (>50 equiv). The concentration of **3** remains constant (>80% of total iron concentration) for a period of time, the duration of which is dependent on the initial concentration of **2** (Figure S8). The concentration of H_2O_2, determined by Raman spectroscopy, during this period shows an exponential decay (Figure 6 and Figure S9). The observed rate constant (k_{obs}) for

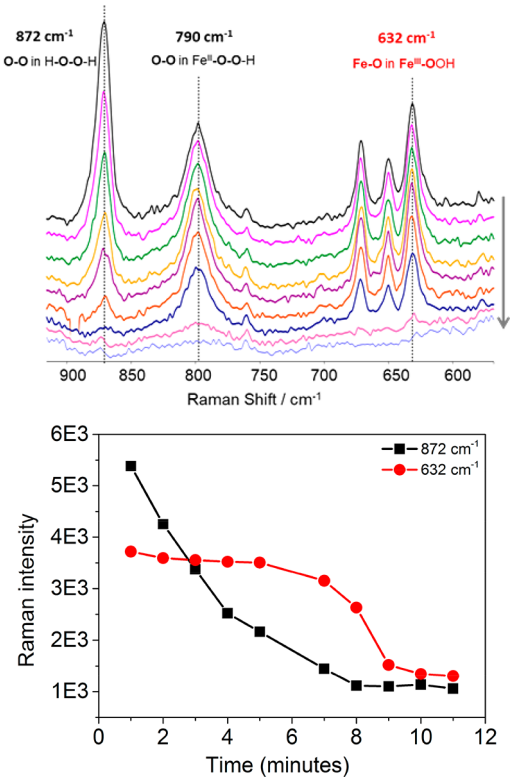

Figure 4. (top) Raman spectra of **1** (ca. 5 mM) in methanol over time after addition of 50 equiv of H_2O_2 at λ_{exc} 785 nm. (bottom) Change in intensity of Raman bands at 872 (of H_2O_2) and 632 cm^{-1} (of **3**) over time at 21 °C. Spectra correspond to the data points shown.

the decomposition of H_2O_2 is linearly dependent on the catalyst concentration (i.e., [**3**], Figure 6), with a second-order rate constant of 0.8 M^{-1} s^{-1} at 21 °C (Figure S9). The rate constant is less than that for the formation of **3** (10.5(±0.1) M^{-1} s^{-1}) and is thus in agreement with **3** as the resting state in the catalytic cycle under steady-state conditions.

Reaction of $[(N4Py)Fe^{IV}{=}O]^{2+}$ (4) with Methanol and H_2O_2. The self-decay rate of **4** (prepared independently),[33] due to reaction with solvent, is low in acetonitrile[30] but is significant in methanol (Figure 7). In methanol, the NIR absorbance of **4** decays exponentially over 1000 s with the concomitant production of 1 equiv of **5a** ($Fe^{III}–OCH_3$) and 0.5 equiv of formaldehyde (see the Supporting Information for details). The kinetic isotope effect for this decay in CD_3OD is ca. 10 (Figure 7).[33] OH/OD exchange does not affect this rate, which is consistent with the competence of **4** in the oxidation of methanol with a rate-determining hydrogen atom abstraction (HAT) step at the C–H bond.

Addition of 1 equiv of H_2O_2 to **4** ($Fe^{IV}{=}O$) in methanol results in conversion to **5a** ($Fe^{III}–OCH_3$) within 200 s, in agreement with data reported in acetonitrile (second-order rate constant of 8 M^{-1} s^{-1} at 21 °C),[30] and is ca. 10 times faster than the reaction of **4** with CH_3OH. However, in stark contrast with the 2:1 ratio of **4** to H_2O_2 required in acetonitrile[30] for full reduction of **4** to the Fe^{III} state, in methanol only 1 equiv of H_2O_2 is required (Figure S10). In both solvents the need for excess H_2O_2 (>0.5 equiv) indicates that H_2O_2 is consumed by other pathways.

$$2[(N4Py)Fe^{IV}(O)]^{2+} + H_2O_2 \rightarrow 2[(N4Py)Fe^{III}(OH)]^{2+} + O_2 \quad (3)$$

DOI: 10.1021/acscatal.8b02326
ACS Catal. 2018, 8, 9665–9674

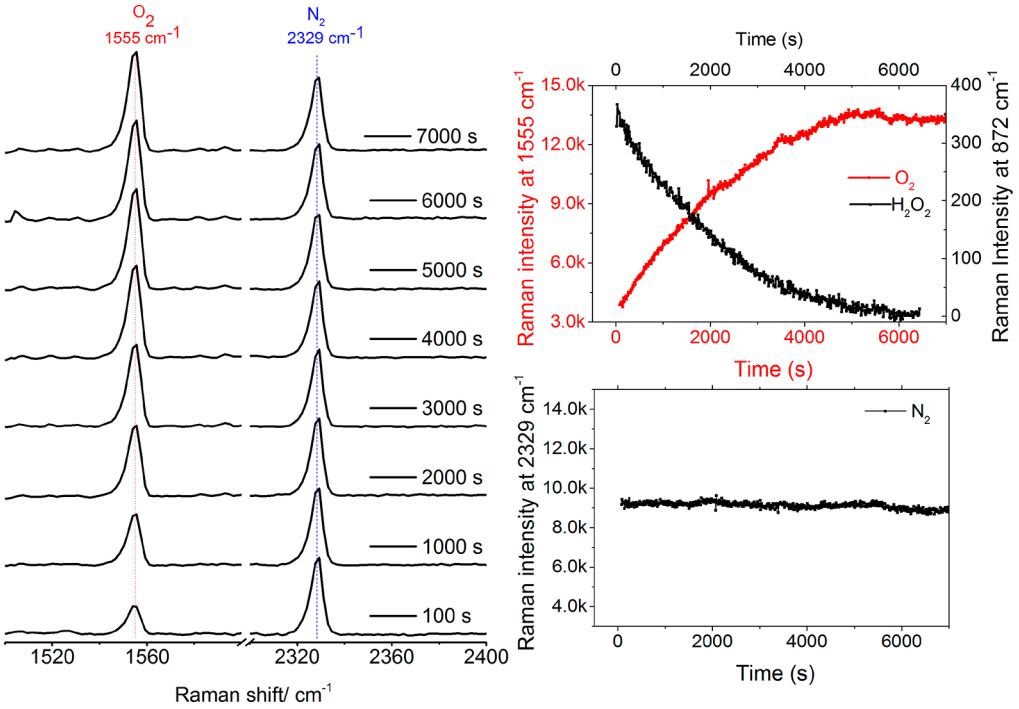

Figure 5. (left) Raman spectra (λ_{exc} 532 nm) obtained from the headspace above the reaction mixture containing **1** (0.25 mM) and 200 mM H_2O_2 in methanol at 21 °C. (right) Change in intensity of Raman band at 1555 cm^{-1} of O_2 (head space, red, λ_{exc} 532 nm, internal reference was 2329 cm^{-1} band of N_2) and at 872 cm^{-1} for H_2O_2 (liquid phase, black, λ_{exc} 785 nm).

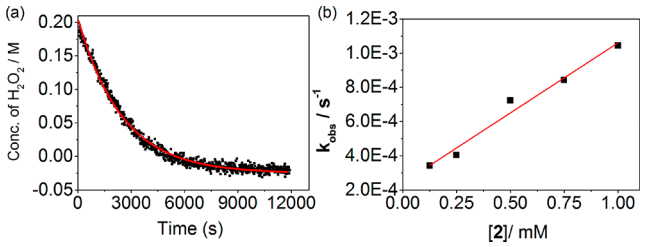

Figure 6. (a) Concentration of H_2O_2 with time following addition of H_2O_2 (200 mM) to **2** (0.25 mM) at 21 °C. (b) Plot of the pseudo-first-order rate k_{obs} versus concentration of **2**.

The OH/D kinetic isotope effect observed in the reduction of **4** with H_2O_2 is masked to some extent by the competing reaction of **4** with CH_3OD (vide supra) but is nevertheless consistent with an HAT mechanism.

In contrast to CH_3OH, in CD_3OD the decay of **4** upon addition of 1 equiv of D_2O_2 is biphasic. Deuterium atom abstraction (from C−D in CD_3OD) by **4** is much slower than the reaction of **4** with 1 equiv of D_2O_2. Consequently, the initial rate (i.e., within 10 min after addition of D_2O_2, 1.13 × 10^{-3} s^{-1}) of decay in the absorbance of **4** is due to reaction with the peroxide only. After this period the rate of decay decreases (to 9.5 × 10^{-5} s^{-1}), which corresponds to the decay of **4** in CD_3OD alone (Figure 7b). A biphasic decay is observed in CH_3OD also but is much less pronounced due to the relatively rapid rate of reaction of **4** with CH_3OD also.

These data indicate that, in addition to reaction with **4**, D_2O_2 is consumed through a second pathway, i.e. by the Fe^{III} species formed initially, which is only apparent when the background reaction of **4** with solvent is slow (i.e., in the case of CD_3OD). The decreased extent of reduction of **4** with 1 equiv of D_2O_2 is similar to that observed in acetonitrile earlier.[30] Although calculation of the KIE for reaction of **4** with H_2O_2/D_2O_2 is estimated as close to 10, indicating that HAT is likely to be rate limiting, the occurrence of several reactions in parallel precludes mechanistic interpretation of this value.

With excess H_2O_2 (40 equiv) in CH_3OH, the characteristic NIR absorbance of **4** disappears over 10 s, while that of **3** (Fe^{III}−OOH, Figure S11) appears concomitantly. These data indicate that the reduction of **4** to **5a** by H_2O_2 is followed by ligand exchange with H_2O_2 to form **3**. Thereafter, the spectral changes are essentially the same as those observed upon addition of H_2O_2 to **2** in methanol.

In summary, the rate of reaction of **4** follows the order H_2O_2 (in CH_3OH) > D_2O_2 (in CH_3OD) > D_2O_2 (in CD_3OD). Notably, the presence of even 1 equiv of H_2O_2 precludes the presence of **4** in methanol, rationalizing the fact that **4** can be observed only when the concentration of H_2O_2 is substoichiometric. The rate of reduction of **4** by H_2O_2 in acetonitrile was reported by Braymer et al.[30] to be insensitive to deuteration (i.e., D_2O_2). In retrospect this observation can be understood by considering the need for an excess of H_2O_2 in that case and the fact that **4** is not the sole species capable of reacting with H_2O_2.

Mechanistic Considerations. The paradigm for oxidation catalysis with complexes such as **2** and H_2O_2 is rapid oxidation to the ferric state and formation of hydroperoxido complexes (e.g., $[(N4Py)Fe^{III}-OOH)]^{2+}$, **3**). Homolytic cleavage of the O−O bond in **3** yields $[(N4Py)Fe^{IV}=O]^{2+}$ (**4**) and a hydroxyl radical, both of which are responsible for oxidation of organic substrates. In the present case, only **3**, and not **4**, is observed in the presence of excess H_2O_2 (Figures 2 and 3), which is consistent with the homolytic cleavage of the O−O bond in **3** being rate determining.

The efficiency in the oxidation of organic substrates is diminished substantially in the presence of excess H_2O_2 due to disproportionation to H_2O and O_2. In the present study, independently prepared **4** is shown to be reduced to the ferric

DOI: 10.1021/acscatal.8b02326
ACS Catal. 2018, 8, 9665−9674

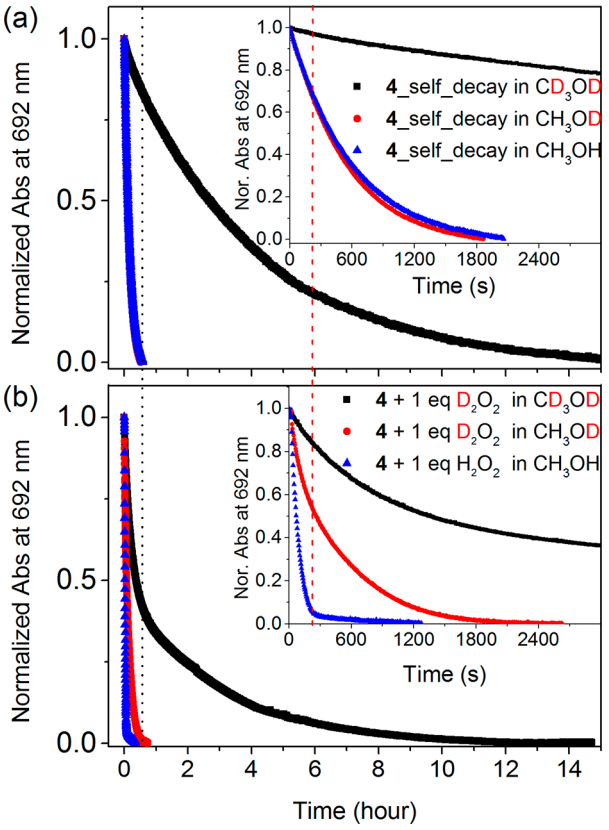

Figure 7. Normalized absorbance of **4** (1 mM) at 692 nm in CH_3OH (blue), CH_3OD (red), and CD_3OD (black) with time in the (a) absence and (b) presence of 1 equiv of D_2O_2. Corresponding UV−vis spectra are shown in Figure S10.

state in methanol rapidly upon addition of H_2O_2. Hence, the fact that **4** is not observed in the presence of excess H_2O_2 can be ascribed to this reaction pathway (b in Scheme 1). Indeed,

Scheme 1. Possible Mechanisms for Reaction of 2 with Excess H_2O_2

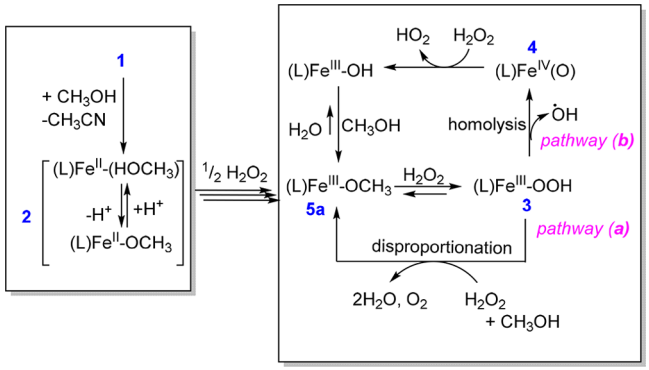

$[(N4Py)Fe^{IV}{=}O]^{2+}$ (**4**) reacts with H_2O_2 (k = 8 M^{-1} s^{-1}) much more rapidly than the observed rate of decomposition of H_2O_2 (k = 0.8 M^{-1} s^{-1}). However, pathway b (Scheme 1) will be kinetically possible only if the rate of the O−O bond homolysis of **3** is sufficiently rapid to account for the rate of decomposition of H_2O_2.

In the present study several observations cast doubt on the validity of pathway b. In methanol, the formation of **4** from **3** is observed once (nearly) all H_2O_2 has been consumed; however, the rate of this reaction is much lower (<3.0 × 10^{-3} s^{-1}, Figure 2) than expected. DFT calculations (vide infra) indicate that the cleavage of the O−O bond is substantially uphill and is accompanied by a low barrier to return to **3** (and hence has an intrinsically substantial thermal barrier). Consequently, the rate of formation of $[(N4Py)Fe^{IV}{=}O]^{2+}$ (**4**) is insufficient to account for the decomposition of H_2O_2 when H_2O_2 is present in excess. This conclusion holds the further consequence that the formation of **4** and hence the oxidation of organic substrates by **4** is not competitive with oxidation of H_2O_2 by **3** (pathway a, Scheme 1). The consequence of this is that the oxidation of organic substrates is only competitive under conditions of low H_2O_2 concentration.

DFT Calculations. The mechanism and comparison of two possible pathways for the reaction of **3** with H_2O_2 were explored through DFT calculations. Geometry optimization and frequency calculations were carried out at the BP86-D_3/TDZP level, with subsequent single point energies at the S12g/TZ2P level, including COSMO-ZORA self-consistently at all stages. All data are given in the Supporting Information.

The doublet ground state calculated for **3** is in accordance with experiment. However, for consistency, the reaction pathways a and b (Scheme 1) were calculated in all three possible spin states: doublet, quartet, and sextet (Figure S12). For both pathways the reaction barriers are much lower in the low-spin state in comparison to those in the other two spin states, and hence the discussion below considers only the low-spin states (Figures 8 and 9).

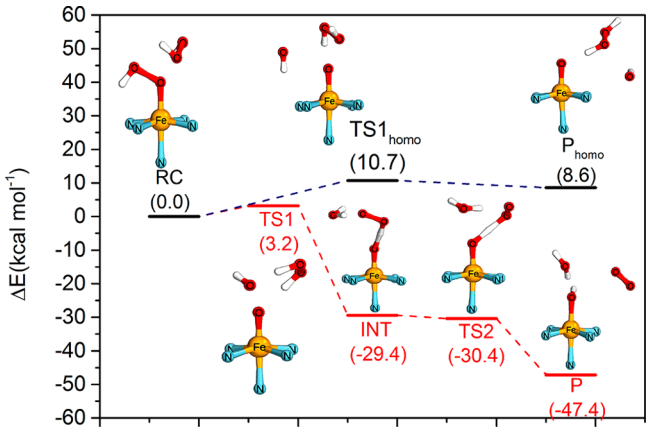

Figure 8. Comparison of energy profiles (in kcal mol^{-1}) of pathway a (catalase, in red) and pathway b (homolysis, in black), as obtained at the S12g/TZ2P//BP86-D_3/TDZP level. (The complete structures indicated in the profile can be also found in Figure 9.)

For the disproportionation pathway a, the reactants, **3** + H_2O_2, initially form a reactant complex (RC) where the peroxide is bound to the iron complex weakly. This step is followed (in TS1) by hydrogen atom abstraction from the peroxide toward the distal OH group of **3**, and simultaneously cleavage of the O−O bond of **3** takes place with a barrier of only 3.2 kcal mol^{-1}. In this TS, the O−O bond in **3** elongates from 1.60 to 2.14 Å, together with a shortening of the H−(OH) distance to 1.45 Å. This is followed by a highly exergonic (−32.6 kcal mol^{-1}) completion of the hydrogen atom transfer process to form H_2O in the intermediate (INT). Simultaneously, the O−O bond of the peroxide shortens from 1.49 to1.35 Å. Formation to the product from INT involves a second hydrogen atom abstraction (barrierless in terms of Gibbs free energy (−1.0 kcal mol^{-1})

DOI: 10.1021/acscatal.8b02326
ACS Catal. 2018, 8, 9665−9674

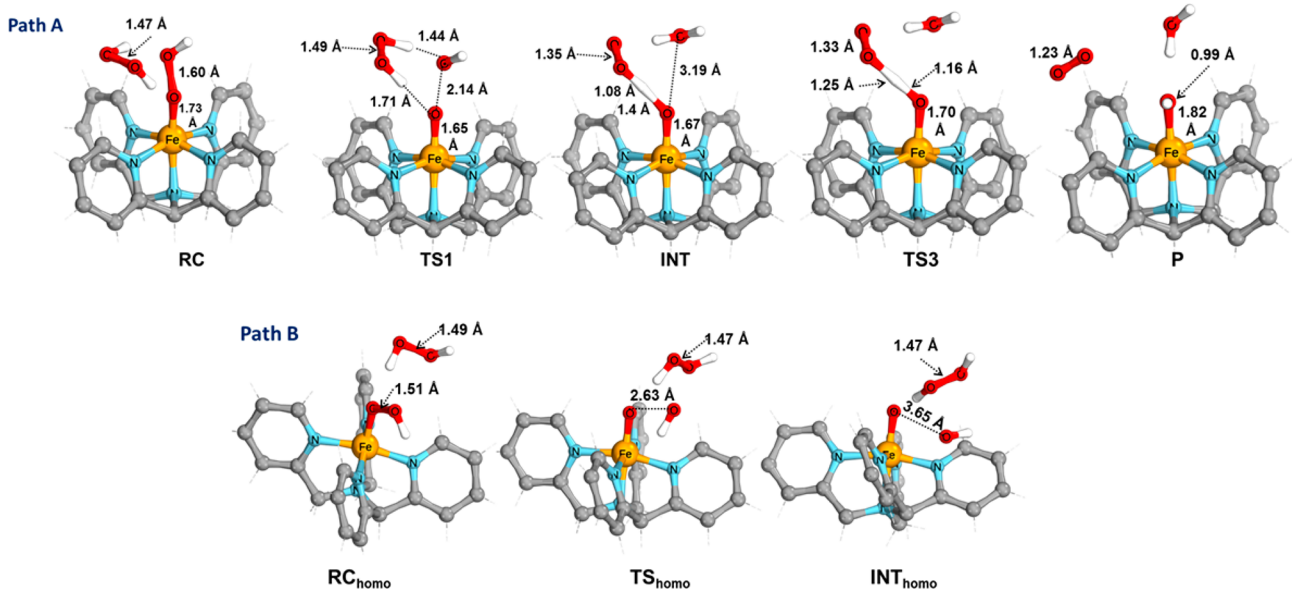

Figure 9. Geometries (bond distance in Å) for key species for both path A (catalase) and path B (homolysis).

and electronic energy (+1.1 kcal mol^{-1})) in which the remaining hydrogen of the peroxide is transferred to the oxygen coordinated to iron. This second HAT is exergonic by ca. −17.0 kcal mol^{-1} and finally leads to the products Fe^{III}−OH + H_2O + O_2.

In contrast, the homolysis pathway b initially forms a similar weakly bound complex in the RC$_{homo}$. However, the activation barrier (10.7 kcal mol^{-1}) for homolytic cleaving of the O−O bond of **3** in TS$_{homo}$ alone to form Fe^{IV}=O is much higher than that in pathway a. The O−O bond in **3** elongates from 1.51 to 2.63 Å with hardly any change in the structure of the peroxide: i.e., the peroxide does not participate actively in the reaction but merely acts as a hydrogen-bond donor. More importantly, the product for this homolytic pathway b, P$_{homo}$, is so close in energy to the TS$_{homo}$ (<2 kcal mol^{-1}) that it readily undergoes the reverse reaction to the initial reactants.

These data are consistent with the observed low rate at which **4** forms from **3** and the rapid consumption of H_2O_2 by direct reaction of **3** with hydrogen peroxide in the disproportionation pathway a.

In summary, there are two pathways that should be considered for the decay of **3**. The first is a unimolecular homolysis to form **4** (Fe^{IV}=O) and a hydroxyl radical. This process is slow and only occurs when the concentration of H_2O_2 is sufficiently low such that it is outside of the solvation sphere of **3**. In this case, both **4** (Fe^{IV}=O) and HO$^{\bullet}$ are eventually formed and are responsible for the oxidation of organic substrates (i.e., methanol), and hence it is a productive reaction.

At higher concentrations of H_2O_2, i.e. where H_2O_2 is likely to be within the solvation sphere of **3**, the formation of two H bonds supports the breaking of the O−O bond of **3**, and either (Scheme 2) (i) stabilizes the formation of **4** ("insertion" of H_2O_2 into the O−O bond of **3**) or (ii) undergoes HAT to form water and HOO$^{\bullet}$ from H_2O_2 and, in a subsequent step, a second HAT from HOO$^{\bullet}$ by Fe^{IV}=O to form [(L)Fe^{III}(OH)]$^{2+}$ (**5b**) and dioxygen.

Our computational data show that the barrier (Scheme 2) to pathway i is substantial and endergonic (10.7 kcal mol^{-1}), even with stabilization through H bonding with H_2O_2. The barrier to pathway ii is much lower (ca. 3.2 kcal mol^{-1}), and leads to

Scheme 2. Homolysis of the O−O Bond in 3 To Form 4 vs Reaction of 3 with H_2O_2

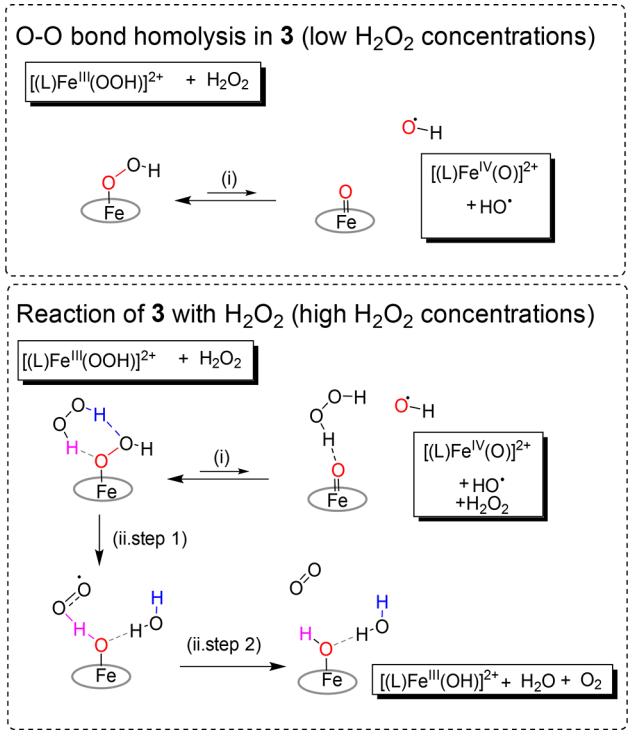

the generation of dioxygen (observed experimentally). Hence, in the presence of H_2O_2, **3** is almost exclusively transformed into **5b**, with subsequent solvent exchange to **5a** (and subsequently through the exchange of methoxido by another H_2O_2 back to **3**). Therefore, in the presence of excess H_2O_2, disproportionation into H_2O and O_2 is the more energetically favored pathway.

Regardless of the pathway, the observed reactivity presents a dichotomy toward the use of complexes such as **2** for oxidation catalysis. **3** (Fe^{III}−OOH) does not appear to react directly with organic substrates (Figure S13),[47] and hence formation of **4** (Fe^{IV}=O) and a hydroxyl radical from **3** through O−O bond

DOI: 10.1021/acscatal.8b02326
ACS Catal. 2018, 8, 9665−9674

homolysis is required. However, both **3** (Fe^{III}–OOH) and **4** (Fe^{IV}=O) react with H_2O_2 more readily than with methanol. Therefore, ideally the steady-state concentration of H_2O_2 should be held as low as possible, yet still sufficiently high to generate **3** and subsequently **4** (Fe^{IV}=O)/HO•. Hence, the rate of addition of H_2O_2 should affect the relative efficiency of **2** in the oxidation of organic substrates, as shown below for the oxidation of methanol.

Competition between the Oxidation of Methanol and H_2O_2 Disproportionation Catalyzed by 2. The oxidation of methanol to methanal occurs concomitantly with the conversion of **4** (Fe^{IV}=O) to $[(N4Py)Fe^{II}–OCH_3)]^+$ (vide supra). However, the rate of this reaction is sufficiently low to exclude it as being an important pathway for **2** in the presence of excess H_2O_2 (i.e., both Fe^{III}–OOH and **4** (Fe^{IV}=O) react much more rapidly with H_2O_2 than with methanol). A number of competing kinetically competent pathways are thus available in the reaction of **2** with H_2O_2, and variation in the steady-state concentrations of reaction components should indicate the relative importance of each of these pathways.

With an 800-fold excess of H_2O_2, ca. 27% of H_2O_2 is disproportionated to H_2O and O_2 (see the Supporting Information for a detailed O_2 concentration calculation), with only 2% generating formaldehyde (Figure 10, bar on the far left). Addition of

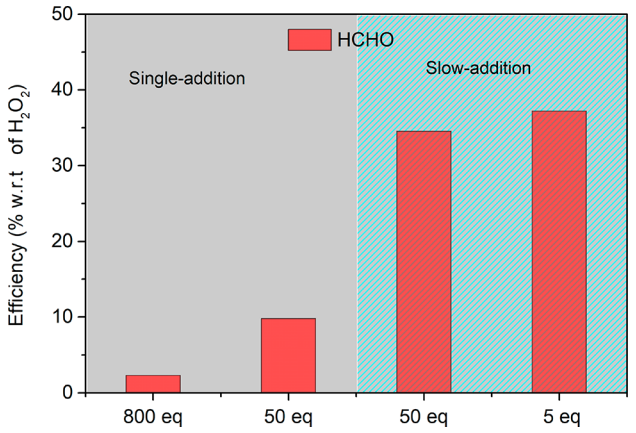

Figure 10. Oxidation of methanol (solvent) with H_2O_2 catalyzed by **1** (0.25 mM). HCHO was quantified colorimetrically (see the Supporting Information for details). The number of equivalents of H_2O_2 is with respect to **2**. *Slow addition* of H_2O_2 indicates a rate of addition of 0.4 equiv min^{-1} (the two rightmost bars).

fewer equivalents of H_2O_2 (second bar from the left) results in a substantial increase in the efficiency in the use of H_2O_2 to oxidize methanol, which increases further by addition of the same amount of H_2O_2 slowly (Figure 10, the two rightmost bars). Adding fewer equivalents slowly over the same time does not increase efficiency further, nor does a change in the concentration of the catalyst (0.25 vs 0.125 mM), since overall conversion rates are controlled by the rate of addition. These data are consistent with the self-decay rate of **4** (Fe^{IV}=O) (vide supra), setting the upper limit for the rate of addition of oxidant to achieve maximum efficiency.

CONCLUSIONS

The species accepted, i.e. Fe^{IV}=O, to be responsible for the oxidation of organic substrates by most non-heme iron catalysts is formed from an Fe^{III}–OOH precursor through O–O bond homolysis, liberating a hydroxyl radical concomitantly. Roelfes and co-workers[3] have noted that, in systems where low-spin Fe^{III}–OOH species are generated (with excess H_2O_2) and observed, the corresponding Fe^{IV}=O species is not observed.

Here we show that, in the case of non-heme N5 coordinated iron complexes that form observable Fe^{III}–OOH species, two key reasons can be invoked to rationalize the absence of a corresponding Fe^{IV}=O species. The first is that, even if it does form, it reacts rapidly and unproductively with H_2O_2 rather than with an organic substrate. Second, and unexpectedly, Fe^{III}–OOH (**3**) reacts more rapidly with H_2O_2 in comparison to the rate that it undergoes O–O bond homolysis to form an Fe^{IV}=O species in the first place.

Ligand exchange, i.e. Fe^{III}–OR to Fe^{III}–OOH (**3**), precedes the oxidation of both organic substrates (eq 2) and H_2O_2 (eq 3). In the present study we show that O–O bond homolysis is relatively slow and is not competitive with the oxidation of H_2O_2 to O_2 by **3**. The reaction bifurcation seen for Fe^{III}–OOH presents a dichotomy in that H_2O_2 must be present in order to form Fe^{IV}=O (**4**), but the steady-state concentration of H_2O_2 should be less than that of Fe^{III}–OOH (**3**), in order that O–O bond homolysis to form Fe^{IV}=O and a HO• radical can take place and hence oxidation of organic substrates to occur. Hence, efficiency with respect to oxidation of organic substrates is increased, as observed in the present study, by maintaining a low steady-state concentrations of H_2O_2.

In conclusion, we show that the oxidation of organic substrates by reactive iron species competes with the reaction of these same species with H_2O_2 and hence wasteful disproportionation of the terminal oxidant. A substantial increase in oxidant efficiency is achieved by maintaining a pseudo-steady-state concentration of H_2O_2 that is below that of the catalyst itself. Furthermore, far from only being a metastable intermediate on route to an Fe^{IV}=O species, the Fe^{III}–OOH complex is kinetically competent in its reaction with H_2O_2. The conclusions reached in the present study have implications with regard to our approach to oxidation catalysis with iron catalysts with pentadentate ligands and in a wider perspective hold implications for the mechanisms invoked for catalase type reactions in both biomimetic and bioinorganic systems.

ASSOCIATED CONTENT

Supporting Information

The Supporting Information is available free of charge on the ACS Publications website at DOI: 10.1021/acscatal.8b02326.

Details of physical and computational methods, additional spectroscopic data, and coordinates for calculated species (PDF)

AUTHOR INFORMATION

Corresponding Author

*E-mail for W.R.B.: w.r.browne@rug.nl.

ORCID

Apparao Draksharapu: 0000-0001-7897-3230
Marcel Swart: 0000-0002-8174-8488
Wesley R. Browne: 0000-0001-5063-6961

Present Address

#A.D.: Department of Chemistry and Center for Metals in Biocatalysis, 207 Pleasant St. SE, University of Minnesota, Minneapolis, Minnesota 55455, United States.

Notes

The authors declare no competing financial interest.

DOI: 10.1021/acscatal.8b02326
ACS Catal. 2018, 8, 9665–9674

■ ACKNOWLEDGMENTS

The COST association action CM1305 ECOSTBio (STSM grant 34080), the European Research Council (ERC 279549, W.R.B.), the labex arcane (ANR-11-LABX-003), MINECO (CTQ2014-59212-P and CTQ2015-70851-ERC, M.S.), Gen-Cat (2014SGR1202, MS), FEDER (UNGI10-4E-801, M.S.), and the Chinese Scholarship Council (CSC) are acknowledged for financial support.

■ REFERENCES

(1) Costas, M.; Mehn, M. P.; Jensen, M. P.; Que, L. Dioxygen Activation at Mononuclear Nonheme Iron Active Sites: Enzymes, Models, and Intermediates. *Chem. Rev.* **2004**, *104* (2), 939−986.

(2) Ghosh, A.; Mitchell, D. A.; Chanda, A.; Ryabov, A. D.; Popescu, D. L.; Upham, E. C.; Collins, G. J.; Collins, T. J. Catalase−Peroxidase Activity of Iron(III)−TAML Activators of Hydrogen Peroxide. *J. Am. Chem. Soc.* **2008**, *130* (45), 15116−15126.

(3) Roelfes, G.; Lubben, M.; Hage, R.; Que, L., Jr.; Feringa, B. L. Catalytic Oxidation with a Non-Heme Iron Complex That Generates a Low-Spin Fe^{III}OOH Intermediate. *Chem. - Eur. J.* **2000**, *6* (12), 2152−2159.

(4) Kim, Y. M.; Cho, K.-B.; Cho, J.; Wang, B.; Li, C.; Shaik, S.; Nam, W. A Mononuclear Non-Heme High-Spin Iron(III)-Hydroperoxo Complex as an Active Oxidant in Sulfoxidation Reactions. *J. Am. Chem. Soc.* **2013**, *135* (24), 8838−8841.

(5) Geng, C.; Ye, S.; Neese, F. Analysis of Reaction Channels for Alkane Hydroxylation by Nonheme Iron(IV)-Oxo Complexes. *Angew. Chem., Int. Ed.* **2010**, *49* (33), 5717−5720.

(6) Park, J.; Lee, Y.-M.; Nam, W.; Fukuzumi, S. Brønsted Acid-Promoted C−H Bond Cleavage via Electron Transfer from Toluene Derivatives to a Protonated Nonheme Iron(IV)-Oxo Complex with No Kinetic Isotope Effect. *J. Am. Chem. Soc.* **2013**, *135* (13), 5052−5061.

(7) Rana, S.; Dey, A.; Maiti, D. Mechanistic Elucidation of C−H Oxidation by Electron Rich Non-Heme Iron(IV)−oxo at Room Temperature. *Chem. Commun.* **2015**, *51* (77), 14469−14472.

(8) Draksharapu, A.; Angelone, D.; Quesne, M. G.; Padamati, S. K.; Gómez, L.; Hage, R.; Costas, M.; Browne, W. R.; de Visser, S. P. Identification and Spectroscopic Characterization of Nonheme Iron(III) Hypochlorite Intermediates. *Angew. Chem., Int. Ed.* **2015**, *54* (14), 4357−4361.

(9) Park, J.; Morimoto, Y.; Lee, Y.-M.; Nam, W.; Fukuzumi, S. Unified View of Oxidative C−H Bond Cleavage and Sulfoxidation by a Nonheme Iron(IV)−Oxo Complex via Lewis Acid-Promoted Electron Transfer. *Inorg. Chem.* **2014**, *53* (7), 3618−3628.

(10) Rohde, J.-U.; In, J.-H.; Lim, M. H.; Brennessel, W. W.; Bukowski, M. R.; Stubna, A.; Münck, E.; Nam, W.; Que, L. Crystallographic and Spectroscopic Characterization of a Nonheme Fe(IV)═O Complex. *Science* **2003**, *299* (5609), 1037−1039.

(11) Nam, W.; Lee, Y.-M.; Fukuzumi, S. Tuning Reactivity and Mechanism in Oxidation Reactions by Mononuclear Nonheme Iron(IV)-Oxo Complexes. *Acc. Chem. Res.* **2014**, *47* (4), 1146−1154.

(12) Cho, K.; Wu, X.; Lee, Y.; Kwon, Y. H.; Shaik, S.; Nam, W. Evidence for an Alternative to the Oxygen Rebound Mechanism in C−H Bond Activation by Non-Heme Fe(IV)═O Complexes. *J. Am. Chem. Soc.* **2012**, *134* (50), 20222−20225.

(13) Kumar, D.; Hirao, H.; Que, L.; Shaik, S. Theoretical Investigation of C−H Hydroxylation by $(N4Py)Fe^{IV}O^{2+}$: An Oxidant More Powerful than P450? *J. Am. Chem. Soc.* **2005**, *127* (22), 8026−8027.

(14) Kaizer, J.; Klinker, E. J.; Oh, N. Y.; Rohde, J. U.; Song, W. J.; Stubna, A.; Kim, J.; Münck, E.; Nam, W.; Que, L. Nonheme $Fe^{IV}O$ Complexes That Can Oxidize the C-H Bonds of Cyclohexane at Room Temperature. *J. Am. Chem. Soc.* **2004**, *126* (2), 472−473.

(15) Sheldon, R. A.; Arends, I. W. C. E.; ten Brink, G.-J.; Dijksman, A. Green, Catalytic Oxidations of Alcohols. *Acc. Chem. Res.* **2002**, *35* (9), 774−781.

(16) Roelfes, G.; Lubben, M.; Hage, R.; Que, L., Jr.; Feringa, B. L. Catalytic Oxidation with a Non-Heme Iron Complex That Generates a Low-Spin FeIIIOOH Intermediate. *Chem. - Eur. J.* **2000**, *6* (12), 2152.

(17) Franke, A.; Van Eldik, R. Spectroscopic and Kinetic Evidence for the Crucial Role of Compound 0 in the P450cam-Catalyzed Hydroxylation of Camphor by Hydrogen Peroxide. *Chem. - Eur. J.* **2015**, *21* (43), 15201−15210.

(18) Solomon, E. I.; Wong, S. D.; Liu, L. V.; Decker, A.; Chow, M. S. Peroxo and Oxo Intermediates in Mononuclear Nonheme Iron Enzymes and Related Active Sites. *Curr. Opin. Chem. Biol.* **2009**, *13* (1), 99−113.

(19) Lehnert, N.; Neese, F.; Ho, R. Y. N.; Que, L.; Solomon, E. I. Electronic Structure and Reactivity of Low-Spin Fe(III)-Hydroperoxo Complexes: Comparison to Activated Bleomycin. *J. Am. Chem. Soc.* **2002**, *124* (36), 10810−10822.

(20) Sam, J. W.; Tang, X.-J.; Peisach, J. Electrospray Mass Spectrometry of Iron Bleomycin: Demonstration That Activated Bleomycin Is a Ferric Peroxide Complex. *J. Am. Chem. Soc.* **1994**, *116* (12), 5250−5256.

(21) Roelfes, G.; Lubben, M.; Chen, K.; Ho, R. Y. N.; Meetsma, A.; Genseberger, S.; Hermant, R. M.; Hage, R.; Mandai, S. K.; Young, V. G., Jr.; Zang, Y.; Kooijman, H.; Spek, A. L.; Que, L., Jr.; Feringa, B. L. Iron Chemistry of a Pentadentate Ligand That Generates a Metastable Fe^{III}-OOH Intermediate. *Inorg. Chem.* **1999**, *38* (8), 1929−1936.

(22) Liu, L. V.; Hong, S.; Cho, J.; Nam, W.; Solomon, E. I. Comparison of High-Spin and Low-Spin Nonheme FeIII−OOH Complexes in O−O Bond Homolysis and H-Atom Abstraction Reactivities. *J. Am. Chem. Soc.* **2013**, *135* (8), 3286−3299.

(23) Decker, A.; Chow, M. S.; Kemsley, J. N.; Lehnert, N.; Solomon, E. I. Direct Hydrogen-Atom Abstraction by Activated Bleomycin: An Experimental and Computational Study. *J. Am. Chem. Soc.* **2006**, *128* (14), 4719−4733.

(24) Faponle, A. S.; Quesne, M. G.; Sastri, C. V.; Banse, F.; de Visser, S. P. Differences and Comparisons of the Properties and Reactivities of Iron(III)−hydroperoxo Complexes with Saturated Coordination Sphere. *Chem. - Eur. J.* **2015**, *21* (3), 1221−1236.

(25) Hirao, H.; Li, F.; Que, L., Jr.; Morokuma, K. Theoretical Study of the Mechanism of Oxoiron(IV) Formation from H_2O_2 and a Nonheme Iron(II) Complex: O-O Cleavage Involving Proton-Coupled Electron Transfer. *Inorg. Chem.* **2011**, *50* (14), 6637−6648.

(26) Li, F.; Van, H. K. M.; Meier, K. K.; Munck, E.; Que, L. Sc^{3+}-Triggered Oxoiron(IV) Formation from O_2 and Its Non-Heme Iron(II) Precursor via a Sc^{3+}−Peroxo−Fe^{3+} Intermediate. *J. Am. Chem. Soc.* **2013**, *135* (28), 10198−10201.

(27) Li, F.; Meier, K. K.; Cranswick, M. A.; Chakrabarti, M.; Van Heuvelen, K. M.; Munck, E.; Que, L. Characterization of a High-Spin Non-Heme Fe(III)-OOH Intermediate and Its Quantitative Conversion to an Fe(IV)═O Complex. *J. Am. Chem. Soc.* **2011**, *133* (19), 7256−7259.

(28) Brown-Marshall, C. D.; Diebold, A. R.; Solomon, E. I. Reaction Coordinate of Isopenicillin N Synthase: Oxidase versus Oxygenase Activity. *Biochemistry* **2010**, *49* (6), 1176−1182.

(29) Quiñonero, D.; Morokuma, K.; Musaev, D. G.; Mas-Ballesté, R.; Que, L. Metal-Peroxo versus Metal-Oxo Oxidants in Non-Heme Iron-Catalyzed Olefin Oxidations: Computational and Experimental Studies on the Effect of Water. *J. Am. Chem. Soc.* **2005**, *127* (18), 6548−6549.

(30) Braymer, J. J.; O'Neill, K. P.; Rohde, J. U.; Lim, M. H. The Reaction of a High-Valent Nonheme Oxoiron(IV) Intermediate with Hydrogen Peroxide. *Angew. Chem., Int. Ed.* **2012**, *51* (22), 5376−5380.

(31) Lubben, M.; Meetsma, A.; Wilkinson, E. C.; Feringa, B.; Que, L. Nonheme Iron Centers in Oxygen Activation: Characterization of an Iron(III) Hydroperoxide Intermediate. *Angew. Chem., Int. Ed. Engl.* **1995**, *34* (13−14), 1512−1514.

(32) Draksharapu, A.; Li, Q.; Logtenberg, H.; van den Berg, T. A.; Meetsma, A.; Killeen, J. S.; Feringa, B. L.; Hage, R.; Roelfes, G.;

DOI: 10.1021/acscatal.8b02326
ACS Catal. 2018, 8, 9665−9674

Browne, W. R. Ligand Exchange and Spin State Equilibria of Fe^{II}(N4Py) and Related Complexes in Aqueous Media. *Inorg. Chem.* **2012**, *51* (2), 900−913.
(33) Chen, J.; Draksharapu, A.; Harvey, E.; Rasheed, W.; Que, L.; Browne, W. R. Direct Photochemical Activation of Non-Heme Fe(IV)═O Complexes. *Chem. Commun.* **2017**, *53* (91), 12357−12360.
(34) McCreery, R. L. *Raman Spectroscopy for Chemical Analysis*; Wiley: 2005; Vol. *225*.
(35) Baerends, E. J.; Autschbach, J.; Berces, A.; Bo, C.; Boerrigter, P. M.; Cavallo, L.; Chong, D. P.; Deng, L.; Dickson, R. M.; Ellis, D. E.; Fan, L.; Fischer, T. H.; Fonseca Guerra, C.; van Gisbergen, S. J. A.; Groeneveld, J. A.; Gritsenko, O. V.; Grüning, M.; Harris, F. E.; van den Hoek, P.; Jacobsen, H.; van Kessel, G.; Kootstra, F.; van Lenthe, E.; Osinga, V. P.; Patchkovskii, S.; Philipsen, P. H. T.; Post, D.; Pye, C. C.; Ravenek, W.; Ros, P.; Schipper, P. R. T.; Schreckenbach, G.; Snijders, J. G.; Solà, M.; Swart, M.; Swerhone, D.; te Velde, G.; Vernooijs, P.; Versluis, L.; Visser, O.; van Wezenbeek, E.; Wiesenekker, G.; Wolff, S. K.; Woo, T. K.; Ziegler, T. *ADF 20016.01*; SCM: Amsterdam, 20016.
(36) te Velde, G.; Bickelhaupt, F. M.; Baerends, E. J.; Fonseca Guerra, C.; van Gisbergen, S. J. A.; Snijders, J. G.; Ziegler, T. Chemistry with ADF. *J. Comput. Chem.* **2001**, *22* (9), 931−967.
(37) Swart, M.; Bickelhaupt, F. M. QUILD: QUantum-Regions Interconnected by Local Descriptions. *J. Comput. Chem.* **2008**, *29* (5), 724−734.
(38) Padamati, S. K.; Angelone, D.; Draksharapu, A.; Primi, G.; Martin, D. J.; Tromp, M.; Swart, M.; Browne, W. R. Transient Formation and Reactivity of a High-Valent Nickel(IV) Oxido Complex. *J. Am. Chem. Soc.* **2017**, *139* (25), 8718−8724.
(39) Becke, A. D. Density-Functional Exchange-Energy Approximation with Correct Asymptotic Behavior. *Phys. Rev. A: At., Mol., Opt. Phys.* **1988**, *38* (6), 3098−3100.
(40) Perdew, J. P. Density-Functional Approximation for the Correlation Energy of the Inhomogeneous Electron Gas. *Phys. Rev. B: Condens. Matter Mater. Phys.* **1986**, *33* (12), 8822−8824.
(41) Grimme, S.; Antony, J.; Ehrlich, S.; Krieg, H. A Consistent and Accurate Ab Initio Parametrization of Density Functional Dispersion Correction (DFT-D) for the 94 Elements H-Pu. *J. Chem. Phys.* **2010**, *132* (15), 154104.
(42) Swart, M. A. New Family of Hybrid Density Functionals. *Chem. Phys. Lett.* **2013**, *580* (0), 166−171.
(43) Swart, M.; Gruden, M. Spinning around in Transition-Metal Chemistry. *Acc. Chem. Res.* **2016**, *49* (12), 2690−2697.
(44) Swart, M.; Rösler, E.; Bickelhaupt, F. M. Proton Affinities in Water of Maingroup-Element Hydrides − Effects of Hydration and Methyl Substitution. *Eur. J. Inorg. Chem.* **2007**, *2007* (23), 3646−3654.
(45) McDonald, A. R.; Que, L. High-Valent Nonheme Iron-Oxo Complexes: Synthesis, Structure, and Spectroscopy. *Coord. Chem. Rev.* **2013**, *257*, 414−428.
(46) Draksharapu, A.; Li, Q.; Roelfes, G.; Browne, W. R. Photo-Induced Oxidation of [Fe^{II}(N4Py)CH_3CN] and Related Complexes. *Dalt. Trans.* **2012**, *41* (42), 13180−13190.
(47) Park, M. J.; Lee, J.; Suh, Y.; Kim, J.; Nam, W. Reactivities of Mononuclear Non-Heme Iron Intermediates Including Evidence That Iron(III)-Hydroperoxo Species Is a Sluggish Oxidant. *J. Am. Chem. Soc.* **2006**, *128*, 2630−2634.

DOI: 10.1021/acscatal.8b02326
ACS Catal. 2018, 8, 9665−9674